Characteristics of electron transport through vertical double-barrier quantum-dot structures: Effects of symmetric and asymmetric variations of the lateral confinement potentials

Dan Csontos* and H. Q. Xu†
Solid State Physics, Lund University, Box 118, S-221 00 Lund, Sweden
(Received 23 May 2002; published 21 November 2002)

We report on a theoretical study of the electron transport through laterally-confined, vertical double-barrier resonant-tunneling (DBRT) structures, defined as one-dimensional (1D)-0D-1D systems, with a tunable lateral confinement. The current and the differential conductance of the systems are calculated and the influence caused by varying the lateral confinement on the device characteristics is investigated. Three representative systems are studied. First of all, a 1D-0D-1D device, symmetric with respect to the current flow, with a variable lateral confinement in the double-barrier quantum-well (DBQW) region, is investigated. This device would in an experimental setup correspond to the structure in which a thin, lateral metallic gate is placed in the DBQW region. Subsequently, calculations are performed for two asymmetric 1D-0D-1D devices, in which the strongest, but varying, lateral confinement is placed either in the collector or in the emitter region. In experiments, these two devices would correspond to the situations where a lateral metallic gate is positioned below or on top of the DBQW structure. The calculations predict several phenomena for the device characteristics. It is shown that as the lateral confinement increases, in addition to those normally observed current onsets and pinch-offs that move toward higher bias voltages, several current onsets and pinch-offs move towards lower bias voltages. These negative shifts of the current onsets and pinch-offs with increasing of the lateral confinement have so far not been expected for gated DBRT devices. It is also found that the threshold voltages, at which the current onsets and pinch-offs appear, depend strongly on the strength and position of the lateral confinement and on the Fermi levels in the collector and the emitter. The models that explain these predictions are presented and discussed.

DOI: 10.1103/PhysRevB.66.205317 PACS number(s): 73.63.Kv, 73.22.Dj, 73.40.Gk

I. INTRODUCTION

Transport through laterally confined double-barrier resonant-tunneling (DBRT) structures has been extensively studied in recent years,[1–31] since the systems have been considered as potential building blocks for multilevel logic and high speed devices in nanoelectronics. Several methods have been developed to realize laterally-confined DBRT structures. These methods have been based exclusively on pregrown DBRT quantum-well structures. The lateral confinements are created by, e.g., etching the structures to columns,[5,14,15,20] ion-beam implantation,[3] and the use of a surface metal gate.[9,11,13,18,19,21] The method of using a surface metal gate is of particular interest, due to the possibilities of tuning the lateral confinement with a voltage applied to the gate and thus of manipulations of the electronic structure in the quantum confined region and the transport properties of the devices. Very recently, an embedded grating metal-gate technique was developed for fabrication of laterally-confined DBRT structures.[22–24,28,31] The technique is very flexible in creating various types of tunable confinements inside as well as outside the DBRT region, such as one-dimensional (1D) emitter and collector. Thus, it becomes possible to experimentally study the effect of the coupling between zero-dimensional (0D) states in the confined region and 1D subbands in the emitter and collector on the device characteristics. There have also been a number of theoretical works in which different aspects of the vertical transport through laterally confined DBRT structures have been treated, including tunneling through 0D states created by the three-dimensional (3D) confinement,[2,8,25,27] charging effects,[4,6,7,10,17] and impurity-assisted tunneling.[16,26]

In this paper we report on a theoretical study of the electron transport through gated vertical DBRT structures. Extensive calculations have been carried out for the devices, and the influence of gate-induced variations of the lateral confinement on the device characteristics has been studied in details. To our knowledge, no such detailed calculations on the development of the characteristics of the gated DBRT devices with continuous variation of the lateral confinement have been reported. The emphasis of our study will be on the electrical properties associated with the vertical symmetry of the devices and the 1D nature of the connecting emitter and collector constrictions. Due to the high degree of complexity of this task, we have restricted our investigation to three distinct cases, for which the qualitative features expected to be observable in the experiments, are extracted. We first study a symmetric, laterally confined DBRT structure (1D-0D-1D structure) corresponding to the experimental situation where a thin metallic confining gate is positioned in the plane of the double-barrier quantum-well (DBQW) region.[18,19,21] Subsequently we investigate two asymmetric, laterally-confined DBRT structures in which the gate is positioned outside the DBRT region, either in the emitter or the collector region (preliminary results for the latter case were presented in Ref. 29). These structures correspond to the devices studied experimentally in Refs. 9,11,23,24,28 and 31. Both the I-V characteristics and the differential conductance spectra have been calculated for the symmetric and the two asymmetric devices with varying lateral confinement. The calculations predict several phenomena for the device char-

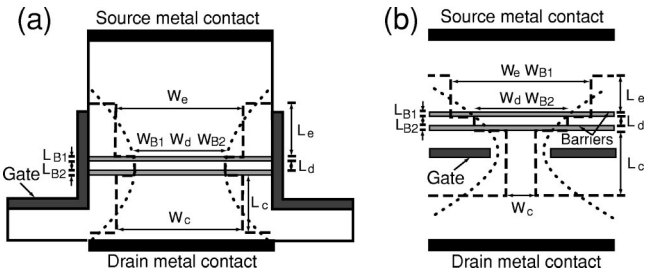

FIG. 1. Schematics of two types of gated, vertical DBRT structures. Dotted lines mark possible depletion regions caused by the gates. Dashed lines illustrate the model potential used in the calculations. (a) A DBRT structure with in-plane gates. (b) A DBRT structure with buried gate, asymmetrically positioned on the collector side of the device.

acteristics. It is found that as the lateral confinement increases, in addition to those current onsets and pinch-offs that move toward higher bias voltages, several current onsets and pinch-offs are found to move toward lower bias voltages. The positive shift of the current onsets and pinch-off with increasing lateral confinement is the phenomenon one normally observes. The negative shift of the current onsets and pinch-offs with increasing lateral confinement has so far not been expected for gated DBRT devices. It is also found that although they are the same in geometric aspects, the two asymmetric, laterally confined DBRT structures show very different device characteristics. The physical origins of all these characteristics will be explained.

The rest of the paper is organized as follows. Section II contains a brief description of the theoretical model and formalism used in the present work. Section III presents the results of the calculations and discussion. Finally, the paper is summarized in Sec. IV.

II. THEORETICAL MODEL AND FORMALISM

The theoretical approach used in the calculations is based on the scattering-matrix method, which was frequently used in recent years for the calculations of electron transport through low-dimensional structures.[16,26,27,29,32,33,34,35] With this method, one can in principle model the electron transport through a device with a given potential profile $V(x,y,z)$ with arbitrary accuracy. In this work we study the effects induced on the device characteristics by a variation of the lateral confining potential, corresponding to the variation of a gate voltage. This means that the current needs to be evaluated as a function of both the source-drain voltage, and the gate voltage and thus the transmission needs to be evaluated as a function of the source-drain voltage, the gate voltage, and the electron injection energy. This is clearly a very difficult numerical task, for a device with a non-uniform lateral confinement potential profile.

For a real device, it is hard to know the exact shape and strength of the lateral confining potential, since both properties depend sensitively on doping profiles, structure parameters, the position of the gate, the voltage applied to the gate, etc. Figure 1 shows schematically possible lateral confinement potential profiles induced by the gates in two gated DBRT structures. As indicated in the figure, depending on the position of the gate, the point of strongest confinement in the structure may occur (i) in the same plane as the DBQW, (ii) on the collector side, or (iii) on the emitter side of the device. The confining potential may, but need not, be symmetric around the point of strongest confinement. Our purpose in this work is to systematically investigate the generic properties of DBRT devices with strong, variable lateral confinement. For this purpose, a simple model structure is used in order to save the computing power. The model structure is schematically indicated by the dashed lines in Fig. 1, where the depletion region is modeled by a stepwise lateral-confining potential profile. Thus our model device consists of five different segments: a 0D region, two thin barriers, a narrow emitter constriction, and a narrow collector constriction. In each segment the potential profile is assumed to be uniform along the direction of transport. However, the geometrical parameters of the different segments, i.e., the length and the lateral width, can be varied independently. In order to further simplify the computational task, we have adopted 2D models as shown in Fig. 1 in the calculations. We have already verified elsewhere[27] the validity of using a 2D model in the analysis of the electron transport through laterally confined vertical DBRT structures.

The electron transmission through such a device is calculated by the scattering-matrix method.[16,26,32,33] In short, the method is a mode-matching method in which the amplitudes of the incoming and outgoing states for a given device are related via a scattering matrix. The device structure may be divided into a number of segments, such that in each segment the potential profile is approximately of transverse dependence only. Thus the motion of the electron in segment, i, can be described by the wave function, $\Psi^i(x,y)$, which satisfies the effective-mass Schrödinger equation

$$\left\{ -\frac{\hbar^2}{2m^*}\left[\frac{\partial^2}{\partial x^2}+\frac{\partial^2}{\partial y^2}\right]+V_c^i(y)\right\}\Psi^i(x,y)=\varepsilon\Psi^i(x,y), \tag{1}$$

where $V_c^i(y)$ is the lateral confining potential in segment i, and m^* is the effective mass (here set to $m^*=0.067m_0$ corresponding to the value for GaAs). The potential $V_c^i(y)$ is assumed to be of square-well type throughout the structure, with the well width in each segment determined by the geometrical parameters defined by the dashed lines in Fig. 1. However, the potential bottoms in $V_c^i(y)$ are different in different segments and depend, in general, on the conduction band offset and the source-drain voltage applied.

In each segment, the transverse part of the electron wave function is expanded in terms of the transverse eigenfunctions, $\phi_m(y)$, of the reservoirs, with the corresponding eigenvalues E_m.[32,36] The expansion coefficients in two adjacent segments, i and $i+1$, are related by means of a transfer matrix $\mathbf{T}(i,i+1)$ which is obtained by imposing the condition of continuity of the electron wave function and its derivative at the interface between the two segments. By iteratively calculating scattering matrices from the source to the drain with the help of the transfer matrices $\mathbf{T}(i,i+1)$, one can obtain the total scattering matrix $\mathbf{S}$, which relates the

amplitudes of the incoming and outgoing states on the two sides of the device. The probability that electrons incident from the source reservoir in the mode $\phi_m(y)$ with energy E and wave vector $k_m^S=[(2m^*/\hbar^2)(E-E_m)]^{1/2}$ will transmit to the outgoing state $\phi_n(y)$ in the drain reservoir can be calculated from

$$T_{nm}=\frac{k_n^D}{k_m^S}|\mathbf{S}_{nm}|^2. \tag{2}$$

The current through the device, at a given bias voltage V and temperature T, may be calculated by means of[35,37]

$$I(\mu_F,V,T)=-\frac{e}{\pi\hbar}\int_0^\infty \sum_{mn}^{R} T_{mn}(E,V)[f_S(E-\mu_F-eV) - f_D(E-\mu_F)]dE, \tag{3}$$

where $f_{S,D}$ are the Fermi distributions in the source and drain reservoir, respectively, μ_F is the chemical potential at the two reservoirs, and R indicates that the summation needs to be done only for those values of m and n for which k_m^S and k_n^D are real. In this work the conduction band offset is set to 0.3 eV, which is appropriate for GaAs/AlGaAs systems, and the potential drop due to the applied bias voltage is assumed to occur across the barriers only, half of it across each barrier.

III. RESULTS AND DISCUSSION

The I-V characteristics and the dI/dV spectra of several devices of the types shown in Fig. 1 have been calculated. In the following we will show the results of the calculations for three devices, a symmetric and two asymmetric 1D-0D-1D systems, with variable lateral confinement. All the three devices have the fixed vertical structure parameters of $L_e=L_c=100$ nm, $L_{B1}=L_{B2}=1$ nm, and $L_d=25$ nm.

A. Resonant tunneling through a symmetric 1D-0D-1D system with varying lateral confinement: Shrinking the lateral size of the dot

We begin with the study of a symmetric 1D-0D-1D device, as shown by the dashed lines in Fig. 1(a). Here we assume that the narrow emitter and collector have a fixed lateral size of $W_e=W_c=100$ nm. However, the lateral size of the DBQW is assumed to be varied in the range of $55 \leqslant W_d, W_{B1}, W_{B2} \leqslant 100$ nm [as schematically indicated in Fig. 1(a)]. The current and differential conductance have been calculated for two different Fermi energies, $\mu_F=4.0$ and 13.0 meV.

In Fig. 2(a) we display the I-V characteristics of the device at $\mu_F=4.0$ meV. The various curves calculated for different lateral confinements are offset for clarity. The figure shows a number of steps or kinks as well as a sharp drop in the current, which all change in bias position with the variation of the lateral confinement. For clarity, we have marked the evolution of the fine features on the upward and downward slopes of the current by solid and dashed lines, respectively. In Fig. 2(b) we show the differential conductance spectra of the device as a function of the bias voltage and the lateral width of the 0D region (defined as the dot width). The solid lines in Fig. 2(b) mark peaks in the differential conductance, which correspond to the current onsets observed on the upward slope of the current shown in Fig. 2(a). The dashed lines, on the other hand, mark negative differential conductance valleys which correspond to the current pinch-offs, i.e., the regions of the downward slope of the current seen in Fig. 2(a).

To understand the physical origin of the fine structure, let us first consider the lowest I-V curve in Fig. 2(a), corresponding to a uniform 1D-0D-1D structure with a lateral width of 100 nm. The curve shows two steps [marked with (1) and (2)] on the upward slope of the resonant current, as well as a sharp downward slope [marked with (3)]. The steps on the upward slope of the current occur at crossings of the 0D states (1,1) and (1,2) with the emitter Fermi level. [Note that in this work, the notation (m,n) refers to a 0D state with the longitudinal quantum number m and lateral quantum number n.] The current drop occurs as the discrete 0D states fall below the cutoff energies of the 1D subbands in the narrow emitter preceding the DBQW. Due to the uniform lateral confining potential, the lateral mode spacing is identical in the 1D narrow emitter and collector, as well as in the 0D region, and only mode-conserving tunneling process is allowed. Thus, all 0D states are pinched-off at the same bias voltage.

As the lateral confinement is increased, the 0D states are pushed up in energy. Correspondingly, the steps or kinks and the sharp downward slope in the current, as well as the peaks and the valleys in the differential conductance, move towards higher bias voltage. It is also seen that the onset and pinch-off of the current associated with the same 0D state increases approximately in parallel with the increase of the lateral confinement. Furthermore, since the lateral confinements in the 1D emitter and the 0D region are no longer identical, the 0D states will be pinched-off at different bias voltages, which can be seen as a splitting of the sharp downward slope in the current (the valley in the differential conductance), marked with (3), into two downward slopes (valleys).

The I-V characteristics and the dI/dV spectra for the same structure, but calculated at $\mu_F=13.0$ meV are shown in Fig. 3. At this Fermi energy, fine features, in the I-V characteristics with a complicated development pattern [Fig. 3(a)] can be observed. The behavior of these fine features is seen even more clearly in the calculated differential conductance [Fig. 3(b)], plotted as a function of the bias voltage and the dot width W_d. Similar to the results in Fig. 2(b), the peaks and valleys in the differential conductance can be attributed to the onsets and pinch-offs of the current associated with the electron transport through individual states in the 0D region. However, at this Fermi energy, we see both features that move toward lower bias voltages and features that move toward higher bias voltages, with the increase of the lateral confinement. For clarity, we have marked the relevant details by solid, dashed, and dotted lines in Fig. 3(b). Those features that move toward lower bias voltages with the increase of the lateral confinement have not previously been reported, to our knowledge, except for a preliminary work we presented in a conference.[29]

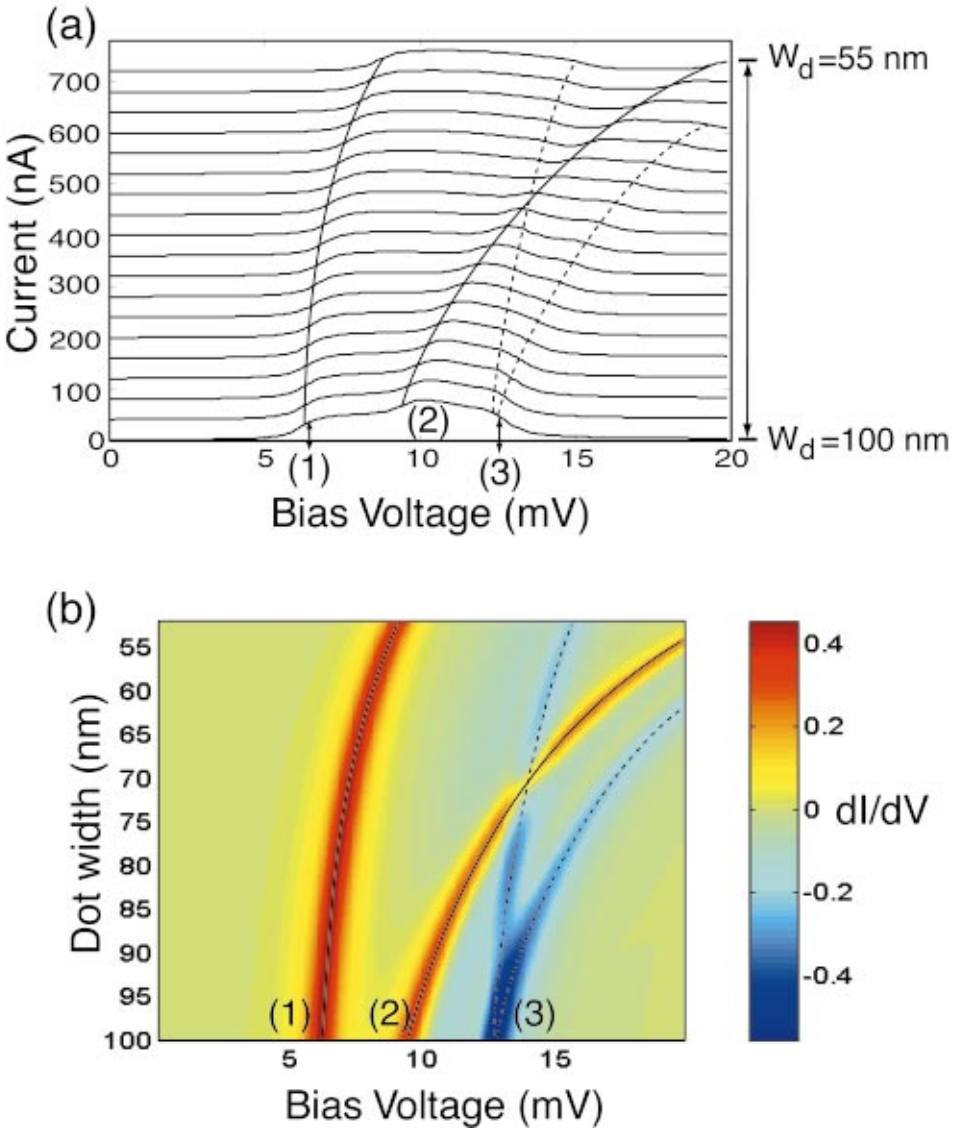

FIG. 2. (Color) (a) *I-V* characteristics calculated at $\mu_F = 4$ meV for a symmetric 1D-0D-1D structure with the geometrical parameters $L_d = 25$ nm, $L_{B1} = L_{B2} = 1$ nm, $L_e = L_c = 100$ nm, and $W_e = W_c = 100$ nm. The widths of the dot and the two barriers are simultaneously varied within the range $55 \leqslant W_d, W_{B1}, W_{B2} \leqslant 100$ nm. The different curves in the figure are plotted for different dot widths and are offset for clarity. The features marked by the solid line with labels (1) and (2) can be attributed to the current onsets through the 0D states (1,1) and (1,2), respectively. The features marked by the dashed lines with label (3) can be attributed to the current pinch-offs through the 0D states (1,1) and (1,2). (b) Differential conductance (color coded) calculated at $\mu_F = 4$ meV for the device as a function of the source-drain bias voltage and the dot width (W_d). The labels (1), (2) and (3) have the same meanings as in (a).

The interpretation of the results in Fig. 3 is the following. At zero bias voltage, the states (1,1), (1,2), and (1,3) are below the Fermi level in the emitter and collector at $W_d = 100$ nm. Thus, in order to have transmission through these states, a large enough bias voltage needs to be applied such that these states are pushed above the collector Fermi level. The associated current steps on the upward slope of the current (as well as the corresponding differential conductance peaks) occur therefore at those bias voltages for which the collector Fermi level is aligned with 0D states. In Fig. 3, the features marked with labels (1), (3), and (4) correspond to the opening of the 0D states (1,3), (1,2), and (1,1) by this mechanism (note that these current steps occur in reverse order compared to the steplike structure expected from the crossings of the emitter Fermi level with the 0D states, as seen in Fig. 2).

As the lateral confinement in the 0D region increases, the 0D states (1,1), (1,2), and (1,3) are pushed up in energy, and move closer to the collector Fermi level at zero bias. The onsets of the current through these states and, hence, the steps and peaks in the current and differential conductance, will therefore successively occur at lower bias voltages [see, e.g., the features marked by dotted lines in Fig. 3(b) for this negative-shift behavior].

At large enough lateral confinements, however, the 0D states (1,1), (1,2), and (1,3) will be pushed above the collector (and emitter) Fermi level already at zero bias voltage. For these confinements, the current onsets will, instead, occur at the alignment of the emitter Fermi level with the 0D states. This yields a positive development of the current onsets, toward a higher bias voltage, with a further increase of the lateral confinement, similar to the behavior of the features seen in Fig. 2. For the 0D state (1,4), which already lies above the Fermi energy of the device with $W_d = 100$ nm at zero bias, the current onset naturally displays this positive-shift behavior from the start [see the features labeled with (2) in Fig. 3].

The downward slope of the resonant current peak displays similarly rich fine structure. The origin of this fine structure is again related to the pinch-offs of the 0D states as they fall below the cutoff energies of the various corresponding 1D subbands in the emitter. The dashed lines with label (5) in

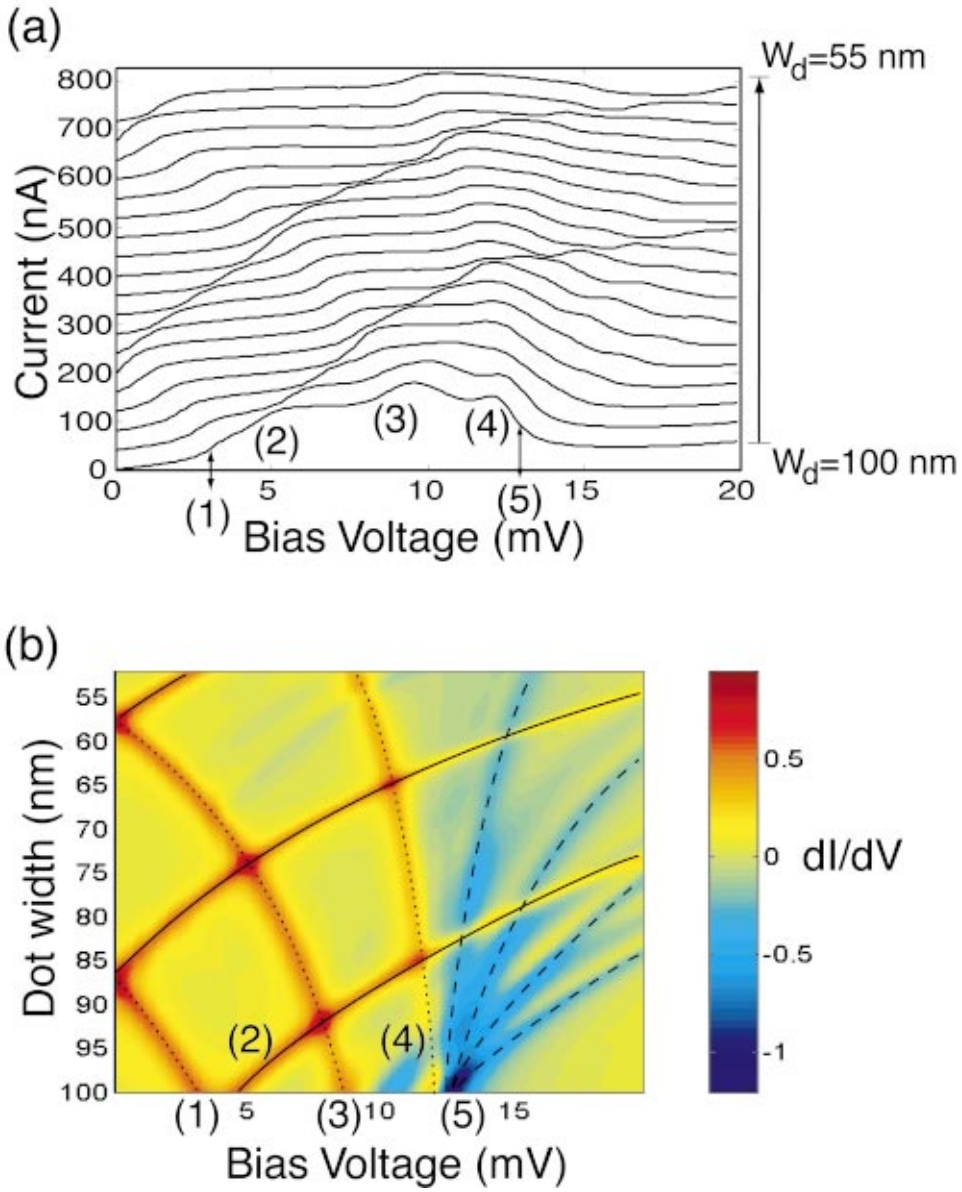

FIG. 3. (Color) (a) *I-V* characteristics calculated at the Fermi energy $\mu_F = 13$ meV for the same symmetric 1D-0D-1D structure as in Fig. 2. The different *I-V* curves in the figure are plotted for different dot widths in the range of $55 \leqslant W_d \leqslant 100$ nm and are offset for clarity. (b) Differential conductance (color coded) calculated at $\mu_F = 13$ meV for the device as a function of the source-drain bias voltage and the dot width (W_d). The features marked with labels (1), (2), (3), and (4) can be attributed to the current onsets through the 0D states (1,3), (1,4), (1,2), and (1,1), respectively. The features marked with label (5) can be attributed to the current pinch-offs through the four 0D states. Also in (b), for clarity, the features corresponding to the current onsets caused by different mechanisms are marked with different types of lines (solid and dotted lines), while the features corresponding to the current pinch-offs are marked with dashed lines.

Fig. 3(b) mark the fine features corresponding to the pinch-offs of the mode-conserving tunneling process. There is, however, an additional weak fine structure on the downward slope of the current. This weak fine structure is associated with the pinch-offs of non-mode-conserving tunneling processes.

B. Resonant tunneling through asymmetric 1D-0D-1D systems with varying lateral confinement: Shrinking the lateral sizes of the narrow collector and the dot

In Sec. III A we studied the electron transport through a laterally confined, symmetric DBRT structure, for which the variation of the lateral confinement occurs only in the DBQW region. We now turn our attention to an asymmetric device in which the narrow 1D collector is subject to the strongest confinement. We will again start with a uniform structure as in Figs. 2 and 3. However, here we will assume that the lateral widths of the 0D region and the second barrier are simultaneously varied in the ranges of $55 \leqslant W_d, W_{B2} \leqslant 100$ nm (W_{B1} is kept fixed at 100 nm) and that the lateral width of the narrow collector is varied in the ranges of $10 \leqslant W_c \leqslant 100$ nm, in such a way that the width of the narrow collector changes twice as fast as the width of the dot ($\delta W_c = 2\,\delta W_d$). In order to make a comparison between the different cases, we again calculate the current and differential conductance at $\mu_F = 4.0$ and 13.0 meV.

The results for $\mu_F = 4.0$ meV are shown in Fig. 4. Similar to the results obtained from the calculations on the symmetric device we observe steps and kinks on both the upward and downward slopes of the resonant tunneling current, and the corresponding peaks and valleys in the differential conductance. For clarity, we have again marked features of interest by solid, dotted and dashed lines in the differential conductance in Fig. 4(b).

A comparison between Figs. 4 and 2 reveals that the observed features are very similar at weak lateral confinements (large lateral dimensions). The features marked by the solid

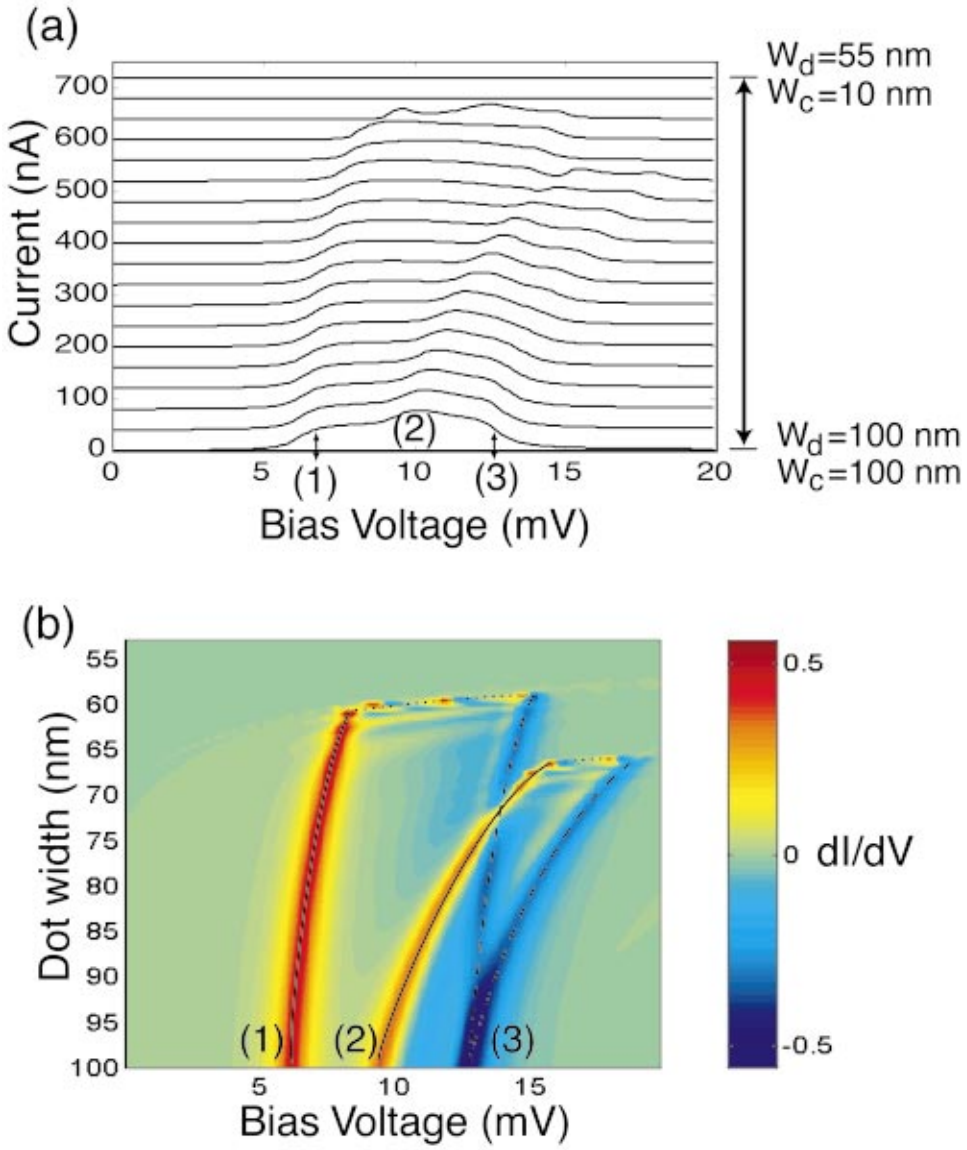

FIG. 4. (Color) (a) I-V characteristics calculated at the Fermi energy $\mu_F=4$ meV for an asymmetric 1D-0D-1D structure with the geometrical parameters $L_d=25$ nm, $L_{B1}=L_{B2}=1$ nm, $L_e=L_c=100$ nm, and $W_{B1}=W_e=100$ nm. The widths of the dot and the second barrier are simultaneously varied within the range of $55\leqslant W_d, W_{B2}\leqslant 100$ nm and the width of the narrow collector is varied within the range $10\leqslant W_c\leqslant 100$ nm, assuming that the width of the narrow collector changes twice as fast as the width of the dot. The different curves are plotted for different dot widths W_d, and for each dot width the corresponding narrow collector width can be calculated from $W_c=2W_d-100$ nm. The curves are offset for clarity. (b) Differential conductance (color coded) calculated at $\mu_F=4$ meV for the device as a function of the source-drain bias voltage and the dot width W_d (with the corresponding lateral collector width $W_c=2W_d-100$ nm). The features marked with label (1) and (2) can be attributed to the current onsets through the 0D states (1,1) and (1,2), respectively. The features marked with label (3) can be attributed to the current pinch-offs through the two 0D states. Also in (b), for clarity, the features corresponding to the current onsets are marked with solid lines, while the features corresponding to the current pinch-offs are marked with dashed lines. The features marked with dotted lines in (b) can be attributed to the current onsets through the 0D states with the mechanism indicated by the schematic shown in Fig. 5(b).

lines with labels (1) and (2) in Fig. 4(b) and the corresponding steps in Fig. 4(a) have the same physical origins as those observed in Fig. 2, i.e., they occur when the 0D states (1,1) and (1,2) cross the emitter Fermi level at certain biases. The features marked by the dashed lines in Fig. 4(b), on the other hand, correspond to the threshold voltages for the pinch-offs of these states. A striking difference between the results shown in Fig. 4 and the results shown in Fig. 2 is seen in the strong lateral confinement region. In this regime, the fine structure associated with the current onsets suddenly shifts very fast toward higher bias voltages until the pinch-offs occur.

This behavior can be understood as follows. Previously, we have seen that the current onsets occur at crossings between the 0D states and the emitter Fermi level (see Fig. 2). In the present case, this is true only if there are available

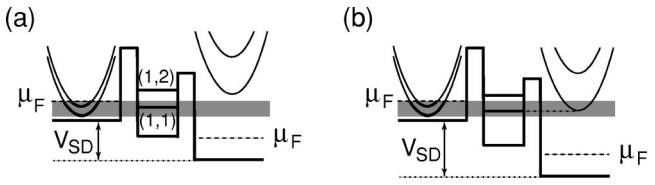

FIG. 5. Schematic views of the conduction band of the asymmetric 1D-0D-1D structure with the strongest lateral confinement assumed in the narrow collector region as studied in Fig. 4. (a) A situation where all the narrow collector subbands have been pushed well above the Fermi energy μ_F in the emitter by the confinement and no current flow through the device is possible. (b) The situation where the 0D state (1,1) is about to open for conduction as it is aligned with the edge of the first subband in the narrow collector. The shaded regions denote the energy window in which electrons are incident from the source (left). Electron flow is possible whenever empty states in both 0D and narrow collector fall into this energy window. μ_F is the Fermi energy in the emitter and collector.

states in the narrow collector region to mediate the transport to the collector reservoir. In the strong lateral confinement regime, this condition is not necessarily satisfied, since the narrow collector subbands can be pushed well above those 0D states which lie below the emitter Fermi level [see schematics of Fig. 5(a)]. Thus a large enough bias voltage is required in this case in order to push the collector states below the 0D states, so that the electron transport through the device again becomes possible. A current onset in this case therefore occurs at the crossing between a 0D state with the edge of the lowest collector subband, to which the 0D state can couple [see schematics of Fig. 5(b) which illustrates the opening of the state (1,1)]. Since the width of the narrow collector constriction is changed faster than the lateral width of the 0D region, the threshold voltage for the current onset in this strong confinement regime will evolve more quickly toward higher bias voltages than in the weak confinement regime [compare the dotted lines with the solid lines in Fig. 4(b)]. Here we should note that at even stronger confinements, the threshold voltage for this type of current onset can eventually exceed the threshold for pinch-off of the associated 0D state, and when this situation occurs the transport through the 0D state is no longer possible. This is clearly depicted in Fig. 4(b) where a dotted line (current onset) and a dashed line (current pinch-off) corresponding to the electron transport through a common 0D state merge together at a point, beyond which no current associated with the transport through that 0D state is observable.

In Fig. 6 we show the current and differential conductance calculated for the same device with the Fermi energy at $\mu_F = 13.0$ meV. Once again, rich fine structure is seen in the I-V characteristics and the dI/dV spectra of the device at this high Fermi energy. However, similarities between the results shown in Figs. 6 and 3 for the current onsets and pinch-off scan still be seen in a large parameter range of the lateral confinement. Thus the majority of the features seen in Fig. 6 can be explained similarly as in Fig. 3, except for the features marked with dotted lines in Fig. 6(b), which can be explained by the same mechanism as for the features marked with dotted lines in Fig. 4(b), using the schematics shown in Fig. 5.

However, it is interesting to note that two fast-moving peaks (the lowest and the uppermost dotted lines) are seen to emerge with an increase of the lateral confinement from the upper solid line in Fig. 6(b). This behavior can be understood as follows. The upper solid line marks the differential conductance peak corresponding to the opening of the 0D state (1,3). This state can couple to both the first and third subbands in the narrow collector due to the possibility of mode-mixing induced by the inhomogeneity in the lateral confining potential of the device (however, subject to the parity-selection rule imposed by the lateral symmetry of the system). With the increase of the lateral confinement, the third subband in the narrow collector will be pushed above the 0D state (1,3). To make the current flow from this 0D state to the third narrow-collector subband possible, a correspondingly higher bias voltage needs to be applied. The first fast-moving conductance peak (the lowest dotted line) seen in Fig. 6(b) corresponds to the evolution of the threshold voltage, which needs to be applied in order to align the state (1,3) and the edge of the third narrow-collector subband, with increase of the lateral confinement. The other fast-moving conductance peak (the uppermost dotted line) corresponds to the evolution of the threshold voltage, which needs to be applied in order to align the state (1,3) and the edge of the first narrow-collector subband, with an increase of the lateral confinement. Evidently, this is an example of mode-mixing effects which in general complicate the fine structure in the device characteristics.

C. Resonant tunneling through asymmetric 1D-0D-1D systems with varying lateral confinement: Shrinking the lateral sizes of the narrow emitter and the dot

To complete our analysis we perform the same calculations for the same structure as in Sec. III B, but under reverse bias. Thus, the point of strongest confinement is assumed to occur on the emitter side of the device. The variation of the lateral confinement of the device is now achieved by varying the lateral width of the narrow emitter within the range of $10 \leqslant W_e \leqslant 100$ nm and the lateral width of the DBQW structure within the range of $55 \leqslant W_d, W_{B1}, W_{B2} \leqslant 100$ nm, in such a way that the width of the narrow emitter is assumed to change twice as fast as the width of the DBQW structure ($\delta W_e = 2\,\delta W_d$). We have again calculated the current and differential conductance for the device at the Fermi energies, $\mu_F = 4.0$ and 13.0 meV.

The results for the current and differential conductance at $\mu_F = 4.0$ meV are shown in Fig. 7, with the dominant features marked again by solid and dashed lines in Fig. 7(b) for clarity. It is seen that at weak lateral confinements, the steps or kinks on the upward slope of the current and the corresponding peaks in the differential conductance obtained for the present case are similar to the results shown in Figs. 2 and 4. Also, these features behave similarly, in the response to the increase of the lateral confinement, to the previous ones. As explained for the previous cases, these current steps and conductance peaks appear at the crossings of the 0D states (1,1) and (1,2) with the emitter Fermi level.

A striking difference between the present device and the devices discussed in Secs. III A and III B lies in the response

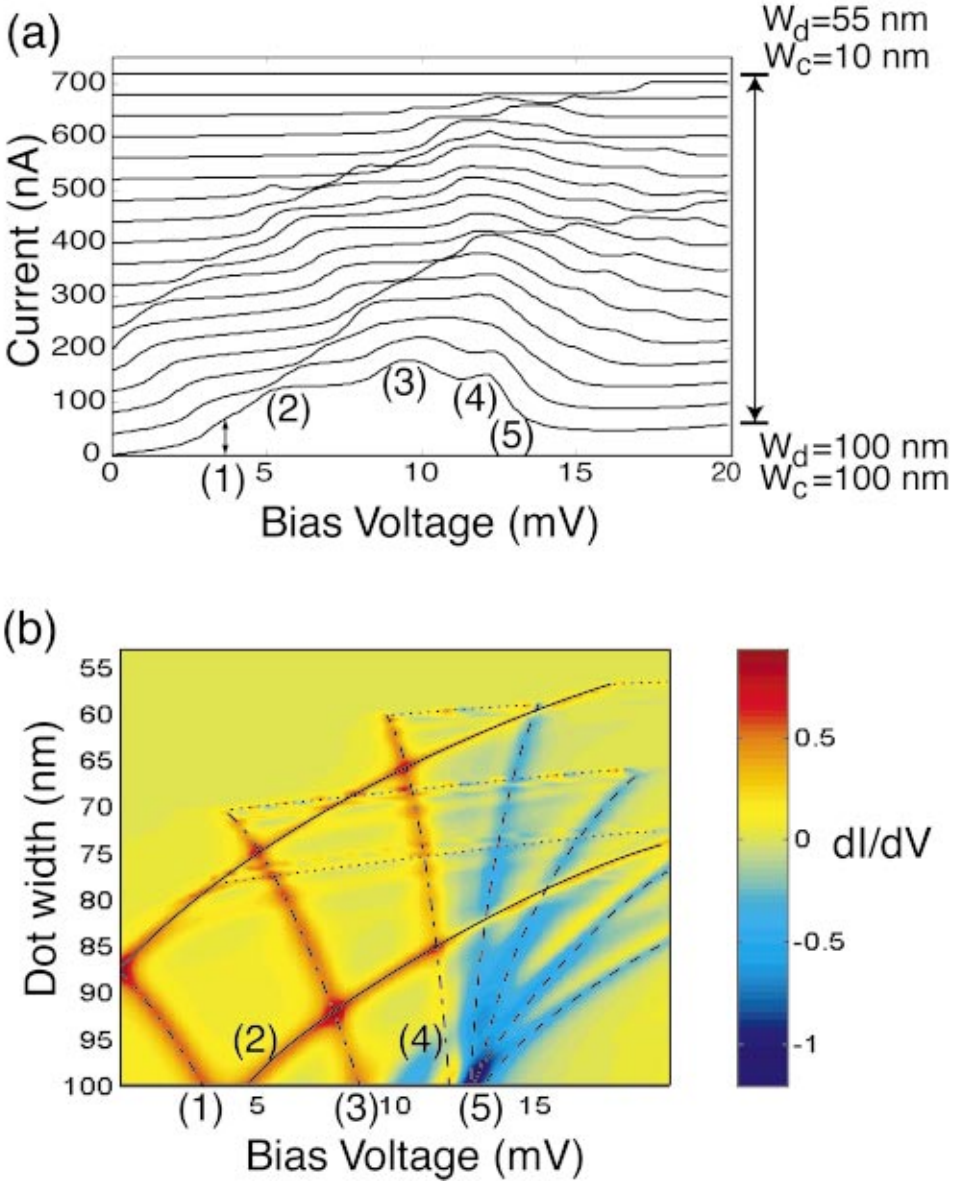

FIG. 6. (Color) (a) *I-V* characteristics calculated at the Fermi energy $\mu_F = 13$ meV for the same asymmetric 1D-0D-1D structure as in Fig. 4. The different curves are plotted for different dot widths W_d, and for each dot width the corresponding lateral collector width can be calculated from $W_c = 2W_d - 100$ nm. The curves are offset for clarity. (b) Differential conductance (color coded) calculated at $\mu_F = 13$ meV for the device as a function of the source-drain bias voltage and the dot width W_d (with the corresponding lateral collector width $W_c = 2W_d - 100$ nm). The features marked with labels (1), (2), (3), and (4) can be attributed to the current onsets through the 0D states (1,3), (1,4), (1,2), and (1,1), respectively. The features marked with label (5) can be attributed to the current pinch-offs through the four 0D states. Also in (b), for clarity, the features corresponding to the current onsets by different mechanisms are marked with different types of lines (solid, dotted and dashed-dotted lines), while the features corresponding to the current pinch-offs are marked with dashed lines. The features marked with dotted lines in (b) can be attributed to the current onsets through the 0D states with the mechanism indicated by the schematic shown in Fig. 5(b)

of the threshold voltages for the pinch-offs of the states (1,1) and (1,2) to the increase of the lateral confinement. Figure 7 shows that with the increase of the lateral confinement, these threshold voltages are shifted towards lower bias voltages [see the sharp downward slope of the current in Fig. 7(a) and the corresponding valleys in the differential conductance marked by dashed lines in Fig. 7(b)]. This is in strong contrast to the previous cases where the threshold voltages for current pinch-offs were seen to develop toward higher bias voltages with increasing the lateral confinement.

This interesting new feature can be understood with the use of the schematics shown in Fig. 8. In Fig. 8(a) we show the band diagram of the device at the threshold voltage for the pinch-off of the state (1,1), i.e., in the condition that the state (1,1) is aligned with the edge of the first subband in the narrow emitter. If the lateral confinement in the narrow emitter is increased, the subbands in the emitter will gradually be pushed up in energy. Thus the threshold voltage for the pinch-off of the state (1,1) is gradually decreased, as indicated in Fig. 8(b). As a result, a negative evolution of the downward current slope and the corresponding differential conductance valley, toward lower bias voltages, is seen with the increase of the lateral confinement. A similar explanation can be given for the negative evolution of the threshold voltage for the pinch-off of the state (1,2) in the device.

Another interesting result seen in Fig. 7 is that as the lateral confinement in the device increases, the threshold voltage for pinch-off of each of the two lowest 0D states and that for the current onset associated with the electron transport through the same 0D state move toward each other. It is also seen that the two types of threshold voltages finally merge together at a certain lateral confinement. With a further increase of the lateral confinement, no electron transport through the considered 0D state is possible (see Fig. 7). This is because, at sufficiently strong lateral confinements, all the subbands in the narrow emitter, which can couple to this

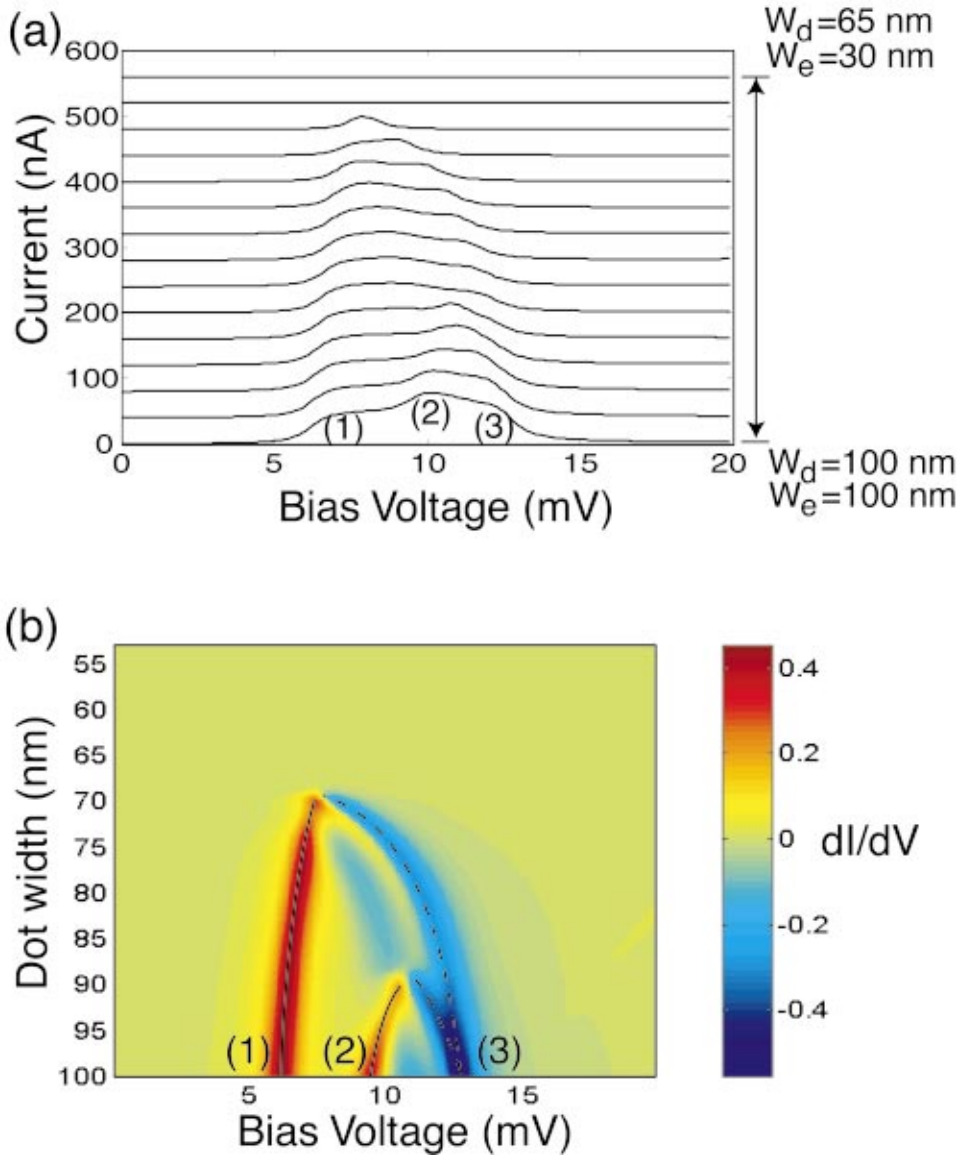

FIG. 7. (Color) (a) *I-V* characteristics calculated at the Fermi energy $\mu_F = 4$ meV for an asymmetric 1D-0D-1D structure with the geometrical parameters $L_d = 25$ nm, $L_{B1} = L_{B2} = 1$ nm, $L_e = L_c = 100$ nm, and $W_c = 100$ nm. The widths of the dot and the two barriers are simultaneously varied within the range of $55 \leqslant W_d, W_{B2}, W_{B1} \leqslant 100$ nm and the width of the narrow emitter is varied within the range of $10 \leqslant W_e \leqslant 100$ nm, assuming that the width of the narrow emitter changes twice as fast as the width of the dot. The different curves are plotted for different dot widths W_d, and for each dot width the corresponding lateral emitter width can be calculated from $W_e = 2W_d - 100$ nm. The curves are offset for clarity. (b) Differential conductance (color coded) calculated at $\mu_F = 4$ meV for the device as a function of the source-drain bias voltage and the dot width W_d (with the corresponding lateral emitter width $W_e = 2W_d - 100$ nm). In both (a) and (b), the features marked with label (1) and (2) can be attributed to the current onsets through the 0D states (1,1) and (1,2), respectively. The features marked with label (3) can be attributed to the current pinch-offs through the two 0D states. Also in (b), for clarity, the features corresponding to the current onsets are marked with solid lines, while the features corresponding to the current pinch-offs are marked with dashed lines.

state, have been pushed above the emitter Fermi level [see the schematic in Fig. 8(c)], resulting in a complete cutoff of the current flow through the device.

Figure 9 shows the calculated current and differential conductance for the device at $\mu_F = 13$ meV. Again, complex features, consisting of peaks, steps, and drops, are seen in the calculated current [Fig. 9(a)], and the corresponding features, consisting of peaks and valleys, are seen in the calculated differential conductance [Fig. 9(b)]. As previously discussed, the 0D states (1,1), (1,2), and (1,3) at $W_d = 100$ nm are below the Fermi level at zero bias and the threshold voltages for the onsets of the current associated with an electron transport through these states are expected to shift towards lower bias voltages with the increase of the lateral confinement. Indeed, the features marked by (1), (3), and (4) in the calculated current and in the differential conductance, which correspond to the opening of the states (1,3), (1,2), and (1,1), are seen to follow the expected behavior with the increase of the lateral

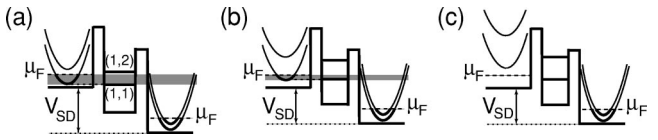

FIG. 8. Schematic views of the conduction band of the asymmetric 1D-0D-1D structure with a strongest lateral confinement assumed in the narrow emitter region as studied in Fig. 7. (a) A situation where the 0D state (1,1) is about to be pinched off as it is aligned with the edge of the first subband in the narrow emitter. (b) Another, but similar, situation where the 0D state (1,1) is about to be pinched off. However, in this situation, the subbands in the narrow emitter have been pushed up in energy and thus the bias voltage required for pinch-off of the state (1,1) becomes lower than that required in the situation (a). (c) A situation where all the subbands in the narrow emitter have been pushed well above the emitter Fermi energy and no current flow through the device is possible. The shaded regions denote the energy windows in which electrons incident from the left may contribute to the current flow. μ_F is the Fermi energy in the emitter and collector.

confinement [see, e.g., the dotted lines in Fig. 9(b)]. The 0D state (1,4) is, however, located above the Fermi energy at zero bias, so that the associated feature marked by (2) in the current and in the differential conductance (the latter also marked by a solid line) are seen to move toward higher bias voltages with the increase of the lateral confinement. Similarly, when the lateral confinement becomes strong enough, the state (1,3) is pushed above the Fermi energy at zero bias and thus the associated feature in the current as well as the associated peak in the differential conductance turn to move toward higher bias voltages with the further increase of the lateral confinement [see the feature marked by the solid line (6) in Fig. 9(b)].

Figure 9 shows also that the threshold voltages for pinch-offs of the lowest four 0D states develop into a fan structure with the increase of the lateral confinement [see the differential conductance valleys marked by dashed lines with label (5) in Fig. 9(b)]. As opposed to that seen in Figs. 3 and 6, the fan structure in the present case is seen to develop toward lower bias voltages. This behavior is similar to the result obtained for the threshold voltages for pinch-off of the two lowest 0D states shown in Fig. 7, and can thus be explained in the same way as for that case in terms of the schematics shown in Fig. 8.

A result seen in the calculation for the device at $\mu_F = 13$ meV is that the features corresponding to the onset of the current associated with the electron transport through the 0D state (1,4), and the related peak in the differential conductance do not vanish, when the edge of the fourth subband in the narrow emitter is pushed above the state (1,4) by the increase in the lateral confinement. This is seen more clearly in Fig. 9(b) where the conductance peak marked by the solid line with label (2) is still visible after crossing the first differential conductance valley, marked by a dashed line, corresponding to the pinch-off of the electron transmission from the fourth subband in the narrow emitter to the state (1,4) in the 0D region. The same behavior is also observed for the features associated with the onset of the current and the related peak in the differential conductance, corresponding to the electron transport through the 0D state (1,3), although it appears at stronger lateral confinements. This behavior is in very difference from that observed in the features associated with the electron transport through the 0D states (1,1) and (1,2) [see the features marked with the labels (3) and (4) in Fig. 9, which show that the current flows through the states (1,1) and (1,2) are completely cut off when the lateral confinement becomes greater than certain strengths]. Furthermore, it is seen in Fig. 9(b) that, after a sudden decrease, the amplitudes of the differential conductance peaks associated with the electron transport through states (1,3) and (1,4), gradually becomes stronger. These behaviors appear as a result of the fact that the coupling of the state (1,3) [(1,4)] in the 0D region to the first (second) subband in the narrow emitter becomes possible when the lateral widths of the 0D region and narrow emitter become different. It should also be noted that the current flows through the dot states (1,3) and (1,4) will eventually be cut off with the increase of the lateral confinement, as clearly exemplified by the feature marked by the dashed line with label (6) in Fig. 9(b). In this example, the current flow through the dot state (1,3) is completely pinched off when the lateral confinements go beyond the values of about $W_d = 60$ nm and $W_e = 20$ nm. This occurs as a result of the fact that, at these strong confinements, the first subband in the narrow emitter has been pushed above the Fermi level and, thus, the current flow through the narrow emitter is no longer possible. Again the features discussed above, as well as other mode-coupling effects, complicate the fine structure observed in the transport characteristics of vertical DBRT structures significantly, and may make the identification of the fine structure very difficult.

IV. SUMMARY

In summary, we have performed a detailed theoretical study of the characteristics of the electron transport through laterally-confined, vertical DBRT structures (defined as 1D-0D-1D systems) with tunable lateral confinements. Such devices have already been achieved in experiments by a selective positioning of gates. Three representative systems have been investigated in this work: a symmetric 1D-0D-1D system with the strongest, but varying, lateral confinement being placed in the 0D region, and two asymmetric 1D-0D-1D systems with the strongest, but varying, lateral confinement being placed either in the 1D collector or in the 1D emitter region. The current and differential conductance of the systems have been calculated using an approach based on a scattering-matrix method.

The calculations reveal that the *I-V* characteristics and the differential conductance spectra of the devices show rich fine structures. Detailed analyses show that the fine structures can be attributed to various onsets and pinch-offs of the current through the devices. The current onsets are found to occur at the crossings between (i) a 0D state and the emitter Fermi level, (ii) a 0D state and the collector Fermi level, or (iii) a 0D state and the edge of a 1D subband in the narrow collector. The current pinch-offs, on the other hand, have been found to occur at the crossings between 0D states and the edges of 1D emitter subbands to which the 0D states can

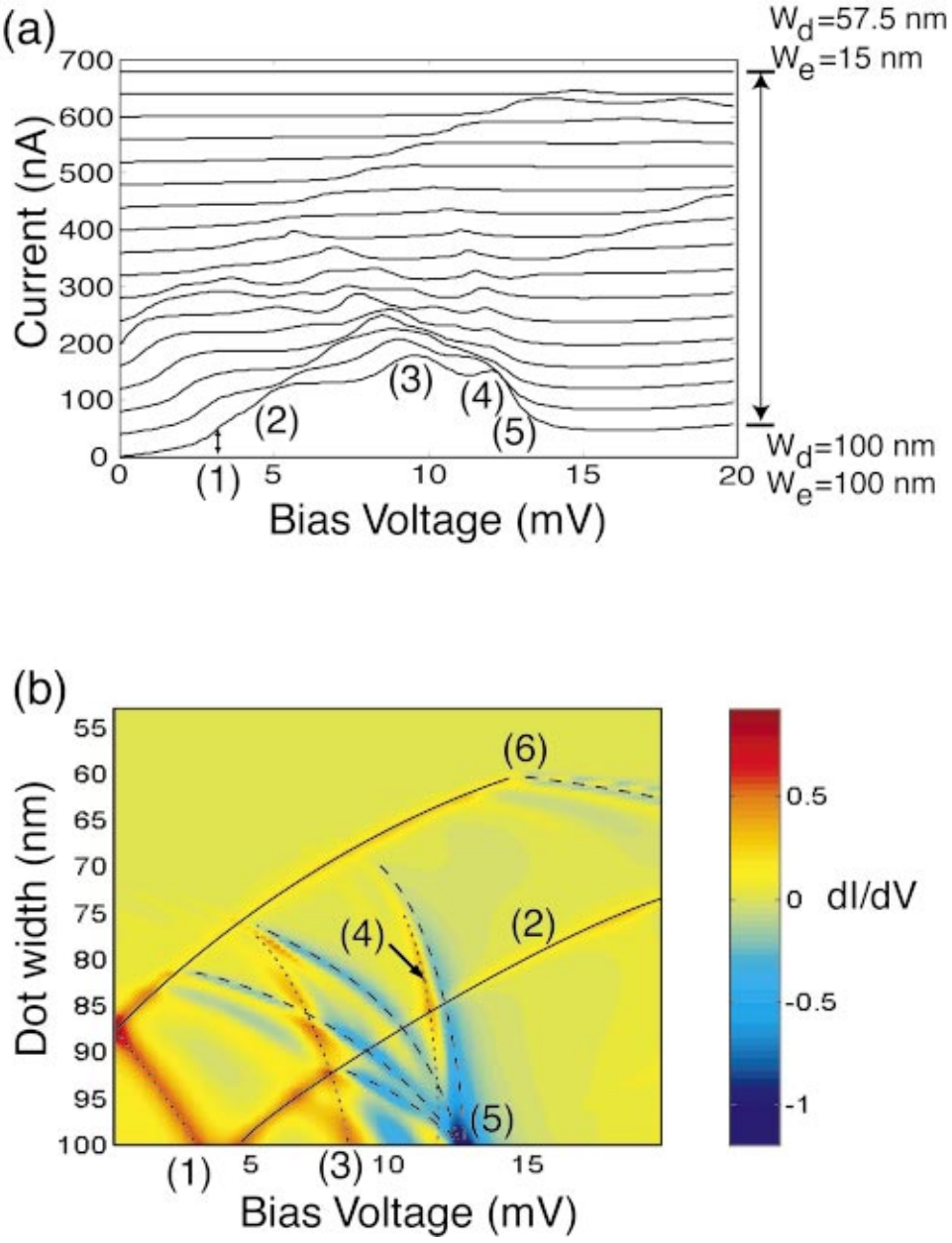

FIG. 9. (Color) (a) *I-V* characteristics calculated at the Fermi energy $\mu_F = 13$ meV for the same 1D-0D-1D structure as in Fig. 7. The different curves are plotted for different dot widths, W_d, and for each dot width the corresponding lateral emitter width can be calculated from $W_e = 2W_d - 100$ nm. The curves are offset for clarity. (b) Differential conductance (color coded) calculated at $\mu_F = 13$ meV for the device as a function of the source-drain bias voltage and the dot width W_d (with the corresponding lateral emitter width $W_e = 2W_d - 100$ nm). The features marked with labels (1), (2), (3), and (4) can be attributed to the current onsets through the 0D states (1,3), (1,4), (1,2), and (1,1), respectively. The features marked with label (5) can be attributed to the current pinch-offs through the four 0D states. Also in (b), for clarity, the features corresponding to the current onsets with different mechanisms are marked with different types of lines (solid and dotted lines), while the features corresponding to the current pinch-offs are marked with dashed lines. The feature marked by the dashed line with label (6) can be attributed to the pinch-off of the current flow by the coupling between the state (1,3) and the first lateral subband in the narrow emitter.

couple. Furthermore, the threshold voltages, at which these current onsets and pinch-offs appear, have been found to depend strongly on the strength and position of the lateral confinement imposed on the devices, and on the Fermi levels in the collector and the emitter.

Most importantly, the calculations have predicted that, as the lateral confinement increases, in addition to those current onsets and pinch-offs that move toward higher bias voltages, several current onsets and pinch-offs are seen to move toward lower bias voltages. These negative shifts of the current onsets and pinch-offs with increasing lateral confinement have not been expected for gated DBRT devices. It is also found that although they are the same in the geometric aspects, the two asymmetric, laterally confined 1D-0D-1D structures show very different device characteristics.

In conclusion, our calculations have predicted various characteristics of electron transport through gated DBRT devices. By varying the lateral confining potentials in the different parts of the devices, the current onsets and pinch-offs of the devices can develop in very different ways. The results presented in this paper provide new understanding on the mechanisms of the electron transport through 1D-0D-1D structures with varying lateral confinements, and should shed light on experimental measurements on the gated vertical DBRT devices, which often show very complicated *I-V* characteristics and differential conductance spectra.

ACKNOWLEDGMENTS

This work, performed within the Nanometer Consortium in Lund, was supported by the Swedish Foundation for Strategic Research (SSF) and the Swedish Research Council (VR).

*Electronic mail: Dan.Csontos@ftf.lth.se
†Electronic mail: Hongqi.Xu@ftf.lth.se

[1] M.A. Reed, J.N. Randall, R.J. Aggarwal, R.J. Matyi, T.M. Moore, and A.E. Wetsel, Phys. Rev. Lett. **60**, 535 (1988).
[2] G.W. Bryant, Phys. Rev. B **39**, 3145 (1989).
[3] S. Tarucha, Y. Hirayama, T. Saku, and T. Kimura, Phys. Rev. B **41**, 5459 (1990).
[4] A. Groshev, Phys. Rev. B **42**, 5895 (1990).
[5] B. Su, V.J. Goldman, M. Santos, and M. Shayegan, Appl. Phys. Lett. **58**, 747 (1991).
[6] A. Groshev, T. Ivanov, and V. Valtchinov, Phys. Rev. Lett. **66**, 1082 (1991).
[7] C.W.J. Beenakker, Phys. Rev. B **44**, 1646 (1991).
[8] G.W. Bryant, Phys. Rev. B **44**, 3782 (1991); **44**, 12 837 (1991).
[9] P. Guéret, N. Blanc, R. Germann, and H. Rothuizen, Surf. Sci. **263**, 212 (1991).
[10] D.V. Averin, A.N. Korotkov, and K.K. Likharev, Phys. Rev. B **44**, 6199 (1991).
[11] M.W. Dellow, P.H. Beton, C.J.G.M. Langerak, T.J. Foster, P.C. Main, L. Eaves, M. Henini, S.P. Beaumont, and C.D.W. Wilkinson, Phys. Rev. Lett. **68**, 1754 (1992).
[12] M.W. Dellow, P.H. Beton, P.C. Main, T.J. Foster, L. Eaves, A.F. Jezierski, W. Kool, M. Henini, S.P. Beaumont, and C.D.W. Wilkinson, Semicond. Sci. Technol. **7**, 442 (1992).
[13] P. Guéret, N. Blanc, R. Germann, and H. Rothuizen, Phys. Rev. Lett. **68**, 1896 (1992).
[14] M. Tewordt, L. Martín-Moreno, J.T. Nicholls, M. Pepper, M.J. Kelly, V.J. Law, D.A. Ritchie, J.E.F. Frost, and G.A.C. Jones, Phys. Rev. B **45**, 14 407 (1992).
[15] B. Su, V.J. Goldman, and J.E. Cunningham, Phys. Rev. B **46**, 7644 (1992).
[16] H. Mizuta, C. Goodings, M. Wagner, and S. Ho, J. Phys.: Condens. Matter **4**, 8783 (1992).
[17] M. Boero and J.C. Inkson, Phys. Rev. B **50**, 2479 (1994).
[18] C.J. Goodings, H. Mizuta, J.R.A. Cleaver, and H. Ahmed, J. Appl. Phys. **76**, 1276 (1994).
[19] S. Tarucha, D.G. Austing, T. Honda, R.J. van der Hage, and L.P. Kouwenhoven, Phys. Rev. Lett. **77**, 3613 (1996).
[20] T. Schmidt, R.J. Haug, K. v. Klitzing, A. Forster, and H. Luth, Phys. Rev. B **55**, 2230 (1997).
[21] S. Tarucha, D.G. Austing, T. Honda, R. v.d. Hage, and L.P. Kouwenhoven, Jpn. J. Appl. Phys. **36**, 3917 (1997).
[22] L.-E. Wernersson, N. Carlsson, B. Gustafson, A. Litwin, and L. Samuelson, Appl. Phys. Lett. **71**, 2803 (1997).
[23] B. Gustafson, N. Carlsson, T. Fukui, A. Litwin, I. Maximov, E.-L. Sarwe, W. Seifert, L.-E. Wernersson, and L. Samuelson, Jpn. J. Appl. Phys. **38**, 343 (1998).
[24] L.-E. Wernersson, M. Suhara, N. Carlsson, K. Furuya, B. Gustafson, A. Litwin, L. Samuelson, and W. Seifert, Appl. Phys. Lett. **74**, 311 (1999).
[25] B. Jouault, M. Boero, G. Faini, and J.C. Inkson, Phys. Rev. B **59**, 4966 (1999).
[26] H. Mizuta, Microelectron. J. **30**, 1007 (1999).
[27] D. Csontos and H.Q. Xu, Microelectron. Eng. **51-52**, 201 (2000).
[28] B. Gustafson, M. Suhara, K. Furuya, L. Samuelson, W. Seifert, and L.-E. Wernersson, Physica E **7**, 819 (2000).
[29] D. Csontos and H.Q. Xu, Jpn. J. Appl. Phys. **40**, 1966 (2001).
[30] L.P. Kouwenhoven, D.G. Austing, and S. Tarucha, Rep. Prog. Phys. **64**, 701 (2001).
[31] B. Gustafson, D. Csontos, M. Suhara, L.E. Wernersson, W. Seifert, H.Q. Xu, and L. Samuelson, Physica E **13**, 950 (2002).
[32] H.Q. Xu, Phys. Rev. B **50**, 8469 (1994).
[33] H.Q. Xu, Phys. Rev. B **52**, 5803 (1995).
[34] D. Csontos and H.Q. Xu, Appl. Phys. Lett. **77**, 2364 (2000).
[35] S. Datta, *Electronic Transport in Mesoscopic Systems* (Cambridge University Press, Cambridge, 1995).
[36] H.Q. Xu, Phys. Rev. B **47**, 9537 (1993).
[37] H.Q. Xu, Phys. Rev. B **47**, 15630 (1993).